A simulation tool to evaluate different capture strategies in a berthing maneuver

(Article begins on next page)

22 December 2024

IMECE2024-144113

A SIMULATION TOOL TO EVALUATE DIFFERENT CAPTURE STRATEGIES IN A BERTHING MANEUVER

Davide Sorli
Politecnico di Torino
Turin, Italy

Martina Ferrauto
Politecnico di Torino
Turin, Italy

Matteo Melchiorre
Politecnico di Torino
Turin, Italy

Pierpaolo Palmieri
Politecnico di Torino
Turin, Italy

Laura Salamina
Politecnico di Torino
Turin, Italy

Stefano Mauro
Politecnico di Torino
Turin, Italy

ABSTRACT

Space operations for satellite maintenance and space debris capture necessitate meticulous design and planning of contact maneuvers, which may include docking or berthing operations. Minimizing contact forces between the chaser and the target is crucial to prevent undesired repulsion or excessive torque demands on the chaser's attitude control system. Various design parameters such as capture strategy, relative speeds, stiffness of components, and force directions influence these maneuvers.

The MUSAPOEM project aims to develop a comprehensive simulation environment for analyzing and designing proximity operations. It focuses on modeling the initial contact phase between spacecraft using a robotic arm for target capture. The simulation tool incorporates detailed models of both spacecraft, of a seven-degree-of-freedom manipulator, and of their mechanical interfaces, with particular attention on the modeling of contact mechanics.

The paper explores different capture maneuvers, evaluating the impact of capture strategy and robot motion planning on the chaser. Simulation results discuss exchanged forces, relative spacecraft motion, energy consumption by the robotic arm and the GNC during the maneuver. Additionally, the robustness of the system is tested throughout various maneuver simulations.

Keywords: on-orbit servicing, robotic system, berthing, multibody

1. INTRODUCTION

In the space exploration landscape, robotics plays a critical role in advancing on-orbit servicing capabilities. The design of robotic systems to perform complex operations such as servicing, refueling and repairing on-orbit satellites requires a detailed understanding of the dynamics of contact in space.

A mechanical coupling is essential for on-orbit servicing missions between the servicer satellite and the target satellite. This coupling can be achieved through two methods: docking or berthing [1]. Berthing is the manual or remotely assisted capture and attachment between two spacecrafts. This process begins with the GNC guiding the servicer vehicle into a rendezvous position, followed by the manipulation of one of the satellites by a manipulator, located on either the chaser or the target spacecraft, directing them towards a common coupling port. The GNC system of the chaser ensures an appropriate relative position between the spacecraft, characterized by a specific pose and zero nominal relative linear and angular velocities. Subsequently, a manipulator installed on either the chaser or the target secures the other vehicle in place. Finally, the manipulator aligns with the corresponding attachment interfaces on the satellites.

A space robotic system (also referred to as space manipulator or space robot) for an IOS mission typically consists of three major components: the base spacecraft (or servicing satellite), an n degree-of-freedom (n-DOF) robot manipulator attached to the servicing satellite, and the target spacecraft to be serviced [2].

The first example of a space robotic manipulator is the Canadarm-1, operated for the first time in the STS-2 mission launched in 1981 [3]. The success of the Canadarm1 demonstrates the usefulness of robotic arm in space, so that the Canadian space agency developed the Canadarm2, equipped on the ISS since 2001 [4]. Canadarm2, with 7-DOFs, is also the first example of redundancy manipulator in space environment.

In recent years other space agencies developed their robotic arms. The European Robotic Arm developed by ESA, installed on the ISS, has a wide handling capability thanks to its 7-DOFs architecture and a range of different end effector to use [5].

The JEM Remote Manipulation System, equipped on the Japanese Experiment module, is specifically designed to support experiments on the JEM Exposed Facility [6].

Robotic systems demonstrate their capabilities in on-orbit servicing and repair operation since the various repairs and upgrade missions on the Hubble space telescope and the assembly of the ISS [7]. In recent years arises mission proposal for operate on-orbit servicing with autonomous robotic systems [8].

The NASA OSAM-1 mission has the purpose to demonstrate the capability of in-orbit assembly operated by a robotic arm (SPIDER) to assemble the satellite communication antenna [9]. The critical review of the mission has been completed in 2022 [10] and independently reviewed in 2024 [11].

The OSAM-2 mission was designed for on orbit manufacturing [12], assisted with a 7-DOFs manipulator designed by Motiv Space systems [13], but unfortunately it was cancelled by NASA in September 2023 due to delays and extra-costs.

Aa example of robotic system proposal for debris removal can be found in [14], where a soft robotic arm (POPUP) architecture is proposed. In [15] the POPUP arm is proposed for on board applications.

A critical aspect of the berthing operation is the contact mechanic between the EE and the target [16], and the forces exchanged between bodies act as a disturbance on the GNC [17]. The dynamic of the space manipulator and the target can be derived from the Kane's formulation [18], which neglects celestial mechanics components and gravitational forces, so that the operation can be considered to be done in free floating condition [19].

The first description of the contact mechanics comes from the Hertzian theory, which the normal contact force is described with an elastic model [20]. To take in account of the energy dissipation the model can be extended to a spring-damper model [21]. A more precise model is the Hunt-Crossley model [17], which include a non-linear damper to take in account different plastic behaviour dependent by the material of contact objects.

In this landscape ASI funded the MUSAPOEM mission, a multi satellite mission to operate autonomous satellite servicing in Earth or Lunar orbit scenario. The mission is designed to be operated by a servicer satellite, assisted with a robotic arm, on a target and non-cooperative satellite. The operation in monitored by a monitoring satellite provided with visual serving systems. The communication with the earth is provided by a communication satellite placed in Earth orbit.

This work presents the design developed for the robotic arm to operate the capture and release maneuvers, the design of the end effector, with a particular attention to the description of the contact mechanics at interface. To study the behaviour of the system during the maneuver it is developed a high fidelity model in a multibody environment. Through a set of simulations, it is demonstrated that the robotic system proposed is capable to realize the maneuver of capture and release, the energy consumption is evaluated, and the drift on the satellite inducted by the maneuver is discussed.

2. MATERIALS AND METHODS

The MUSAPOEM project involve the study of autonomous berthing and docking operation performed in a multi-satellite mission scenario. This work considers the case of a berthing operation performed by a robotic arm mounted on the Servicer satellite (chaser) to reach the target satellite, which is non-collaborative.

2.1 Robotic arm physical model

The robotic arm task is to perform capture and release operation of a target satellite with a mass of about 500kg. The arm is mounted on a bigger servicer satellite (chaser), with a mass of 2000kg, FIGURE 1. The sizes and the operation condition are comparable to other planned missions, in particular the mission used as reference is OSAM-2 [12].
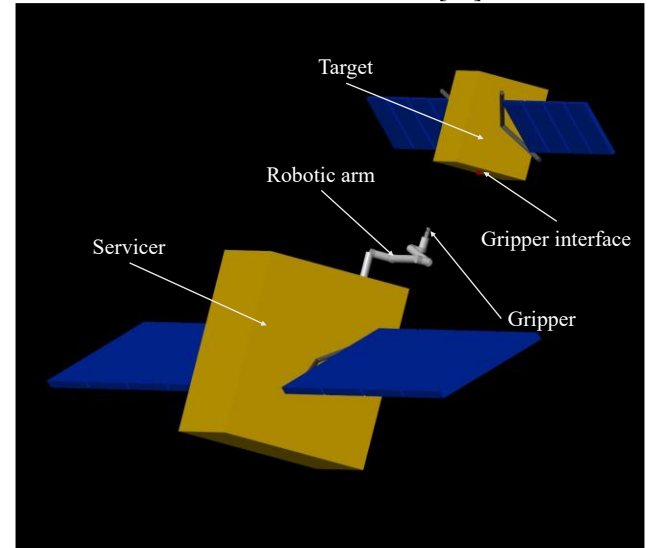

FIGURE 1: ARCHITECTURE OF THE MISSION

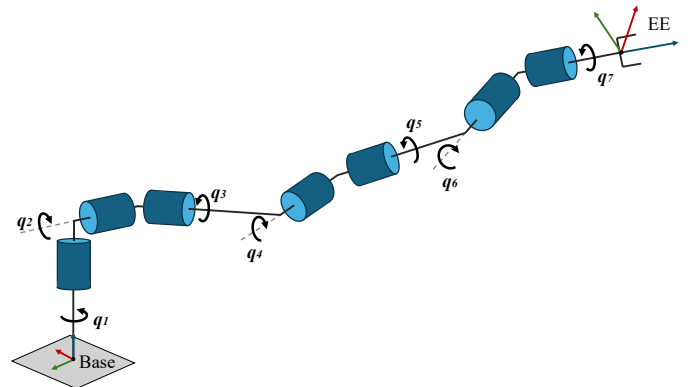The robot kinematic of the arm developed is shown in FIGURE 2.

FIGURE 2: ROBOT KINEMATIC

The robot arm is modeled applying the rigid body model approach (RBM) in Simscape Multibody™ environment.

2.2 End effector model and interface

The end effector design is crucial to accurately achieve the capture of the target satellite. The end effector must maintain the contact with the interface on the target for the whole berthing and unberthing maneuver. Space manipulators can have different type of end effector, it mainly depends on their job requirements and the size of the manipulator and the satellites involved. For the MUSAPOEM project, the size of the manipulator and the servicer and target masses are comparable to some actual mission such as OSAM-2, which use a gripper type end effector. It is designed a gripper end effector dedicated for the MUSAPOEM project. The mechanism is based on a parallelogram architecture, to maintain the parallel constraint between the two fingers, which allows to maintain the orientation information between gripper and interface. Dimensions of the mechanism are chosen to achieve the necessary friction force with a low torque application by the actuator. The interface on the target side is modeled with a simple cube. Final design of the end effector is shown in FIGURE 3.
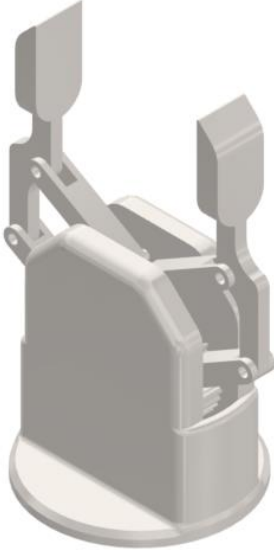

FIGURE 3: END EFFECTOR DESIGN

2.3 Contact Mechanics

An accurate description of the contact mechanic between EE and interface is important to accurately understand the behaviour of the system composed by the two satellites during the robotic manipulation maneuver. Contact mechanics in space environment is a theme investigated in literature, and the choice of the model to be used may depend by the application, the simulation condition, the software used. The use of multibody approach to simulate and verify this kind of operations is a well-established practice [22], [23], [24]. The simulation environment used for this work is Simscape Multibody™ . In this environment contact between flexible bodies can be analysed both with build-in models or by tools developed ad hoc [25]. An issue that arises in contact simulations is often represented by the low time step needed to calculate the contact forces in case of complex geometries or complex contact conditions. In this work it is simulated the whole capture and release maneuver in space

environment, which is performed during a time of about 600 second. This kind of simulation needs to introduce some simplification in the contact mechanics description. For the case presented, the EE and the interface contact should be described as a plane-plane contact, however this contact condition is quite expensive for the software to simulate. The solution proposed in this work is to introduce in the model some contact proxies, represented as spheres fixed on the EE fingers, FIGURE 4, to reconduct the contact to a sphere-plane case, much more efficient to calculate with a significative speed up of the simulation.
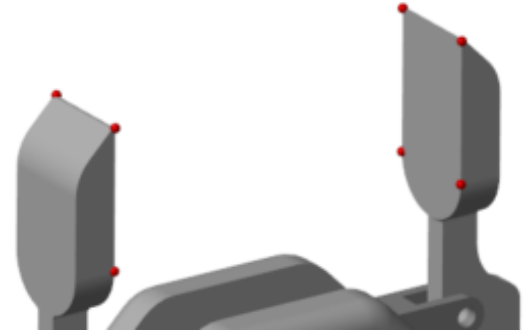

FIGURE 4: DETAIL OF THE CONTACT PROXIES

With this simplification, the contact force expressed during the contact is divided on the four contact proxies, so the total force is the sum of the forces on the proxies.

The contact model used to calculate the normal contact force is defined by an elastic component, coming from the Hertzian contact theory, and by a damping component, which takes into account the energy dissipation during contact. The third parameter is the depth of contact, which is used to maintain a continuous damping coefficient during the contact, avoiding computation issues given by the discontinuity of contact.

Usually the determination of these parameters is non-trivial, since they depend on the material and the geometry of contact elements, and in the case of complex geometries contact parameters may not be constant during simulation. However, since the simplification proposed to describe contact, the behaviour is reducible to the sphere-plane case. For this simplified case, the calculation of the contact stiffness coefficient is straightforward from the Hertzian theory [17]:

$$k(q) = \frac{cE_1E_2}{E_1(1-v_2^2)+E_2(1-v_1^2)}a(q) = c \cdot a(q)E^* \quad (1)$$

where E_1, E_2 are the Young's modulus of the materials constituting the contact bodies, v_1, v_2 are their Poisson's ratios, c is a load dependent coefficient equal to 4/3 for the sphere-plane case. $a(q)$ is the active radius of the contact surface area, for the sphere-plane case it is computed as:

$$a = \frac{3F_nR}{4E^*} \quad (2)$$

where R is the radius of the proxy sphere, F_n is the normal contact force.

With the proposed EE design it is possible to control the normal contact force expressed at the interface by controlling the torque applied on the mechanism. In presence of friction, the normal force must be enough to generate a friction to maintain adhesion condition between EE and interface. In adhesion condition, the friction force F_t is equal to the inertia of the target, which is known because of the motion law of the end effector applies a known maximum acceleration, and the mass of the target is defined. So the normal force can be computed assuming a friction coefficient of stiction. With the above dissertation it is possible to determine the contact stiffness coefficient $k = 1.32 \cdot 10^5 \, N/m$. The damping coefficient is trickier to define because of its intrinsic nonlinearity that try to describe the plastic deformation of the material. A precise estimation can be done with experimental analysis coupled with parameter influence analysis, which is not possible at this stage of the project. However, literature references [26], [27] suggests a value which is 3 order of magnitude lower that the stiffness coefficient. In the case presented, the damping coefficient value assumed is $d = 1.32 \cdot 10^2 \, Ns/m$.

The friction model is a Coulomb friction based method, updated to maintain the friction coefficient constant during the developing of the contact. The model is defined by three parameters, a friction dynamic coefficient, a stiction friction coefficient and a critical velocity that identify the condition of maximum friction. In the case presented, where the contact is basically in static condition, the critical velocity is set to a low value of $V_c = 5 \cdot 10^{-4} \, m/s$, to have a precise description of the stiction phase.

The material which is assumed to be used for the building of the contact bodies is 7075 Aluminum alloy. In **TABLE 1** they are highlighted the dimensions assumed to define the contact model parameters:

TABLE 1: VALUES ASSUMED TO DEFINE THE CONTACT MODEL PARAMETERS

Properties	Symbol	Values
Elastic modulus (GPa)	E	72
Poisson's ratio	ν	0.33
Proxy sphere radius (mm)	R	1
Stiction coefficient	μ_s	0.5
Friction coefficient	μ_d	0.35

2.4 Control strategy

The MUSAPOEM mission scenario starts with the chasing of the target satellite from some kilometer of distance to the berthing capture. In this work the phase of the mission to be simulated is the latter, without including the whole process of identifying the target satellite, approaching and aligning. So the starting condition for the berthing operation is of target and servicer having null relative velocity. The maneuver considered involves three phases. The first phase involves the approaching of the robot arm to the target. The second phase involves the grasping performed by the EE. The last phase completes the berthing operation with the joining of the servicer and target. The maneuver is carried out in reverse in case of unberthing maneuver. The target identification and pose estimation is performed using a camera system mounted on the chaser, which gives the pose of the target with respect to the base of the robot. Reference of this approach for similar application are found in [28], [29]. The GNC of the servicer can maintain the pose of the servicer stable during the operation. The robotic arm operations causes disturbances on the GNC system, and the GNC system cause a disturbance on the robotic arm. The state of the robot in the joint space is assumed to be always available due to direct measurement of encoders mounted on the joints. The target pose is assumed to be always available, in the hypothesis that the camera system can always identify the target and the interface.

The pose to be reached by the end effector $\boldsymbol{x}_s = [\boldsymbol{p}_s, \boldsymbol{\phi}_s]^T$ is determined by the visual servoing. The current pose of the EE is computed through the forward kinematics. The definition of the velocity set involves the solving of the position and the orientation problem.

The algorithm proposed solve them separately. The position error is computed as:

$$\boldsymbol{e}_p = \Delta \boldsymbol{p} = \boldsymbol{p}_s - \boldsymbol{p}_{fb} \qquad (3)$$

Where $\boldsymbol{p}_s$ is the position to be reached, and $\boldsymbol{p}_{fb}$ is the current position of the target. From the position error it is calculated the desired velocity of the end effector, choosing a trapezoidal profile. The velocity profile set $\dot{\boldsymbol{p}}_s$ is defined as follows:

$$\dot{\boldsymbol{p}}_s = \min\left(a_o t, v_o, \sqrt{2a_0 \|\Delta \boldsymbol{p}\|}\right) \frac{\Delta \boldsymbol{p}}{\|\Delta \boldsymbol{p}\|} \qquad (4)$$

Where $a_o = 0.0005 m/s^2$ is the maximum acceleration, $v_o = 0.01 m/s$ is the maximum velocity for the end effector.

A similar approach is used to solve the angular problem. The orientation error is defined using the quaternion representation $Q = \{\eta, \boldsymbol{\epsilon}\}$:

$$\boldsymbol{e}_O = \Delta \boldsymbol{\epsilon} = \eta_{fb}(\boldsymbol{q})\boldsymbol{\epsilon}_s - \eta_s \boldsymbol{\epsilon}_{fb}(\boldsymbol{q}) - S(\boldsymbol{\epsilon}_s)\boldsymbol{\epsilon}_{fb}(\boldsymbol{q}) \qquad (5)$$

The desired angular velocity is computed with the same criteria:

$$\dot{\boldsymbol{\phi}}_s = \min\left(\alpha_0 t, \omega_o, \sqrt{2\alpha_0 \|\Delta \boldsymbol{\epsilon}\|}\right) \frac{\Delta \boldsymbol{\epsilon}}{\|\Delta \boldsymbol{\epsilon}\|} \qquad (6)$$

Where $a_o = 0.0005 rad/s^2$ is the maximum angular acceleration, $v_o = 0.01 rad/s$ is the maximum angular velocity for the end effector. The typical module of velocity profile obtained with this method is shown in FIGURE 5.
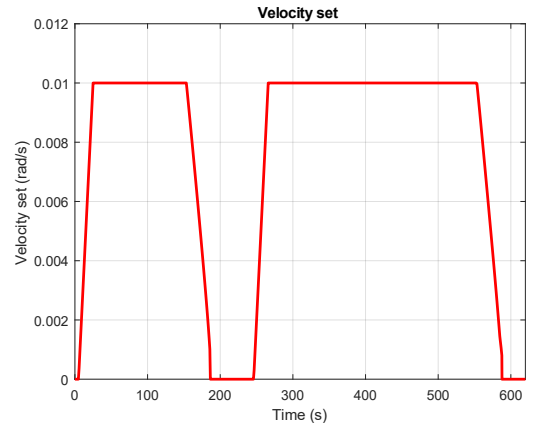

FIGURE 5: TYPICAL VELOCITY PROFILE

Using the vector of desired velocity $v_s = [\dot{p}_s, \dot{\phi}_s]^T$, calculated from the error $e = [e_p, e_o]^T$, the set of joint velocities are calculated by performing the inverse differential kinematics:

$$\dot{q}_d = J^\dagger v_d \qquad (7)$$

where

$$J^\dagger = J^T (J \cdot J^T)^{-1} \qquad (8)$$

is the right pseudo inverse of the Jacobian matrix J. With this formulation, the redundancy of the manipulator, given by the 7th DOF is used to locally minimize the norm of the joints velocities [30].

3. RESULTS AND DISCUSSION

The multibody simulation tool has been tested throughout a series of analysis, evaluating the capability of the robotic arm to perform the capture and release maneuvers. The phases of the berthing maneuver are shown in FIGURE 6, the phases of the unberthing maneuver are shown in FIGURE 7.

The control strategy proposed has been tested, the output of the simulation tool allows to evaluate the energy consumption of the robotic arm during the maneuver. It has been tested also the condition of no GNC intervention during the capture and release, to verify that the manipulator can accomplish the maneuver even if the servicer is in free floating condition.
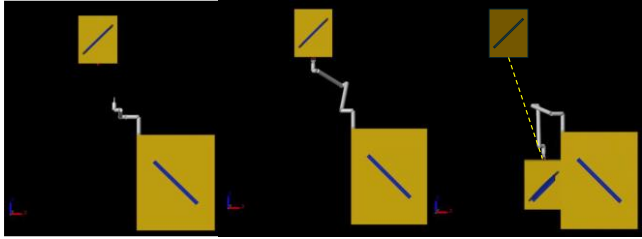

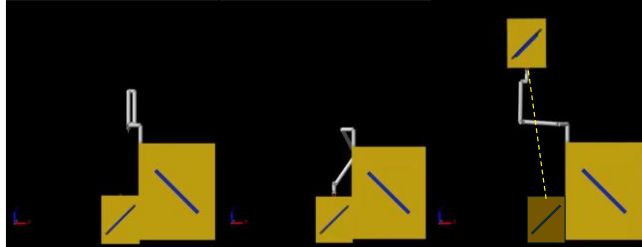**FIGURE 6:** PHASES OF THE BERTHING MANEUVER

FIGURE 7: PHASES OF THE UNBERTHING MANEUVER

In FIGURE 8 is shown the comparison of contact forces expressed at the interface between target and EE in case of intervention of GNC or its absence during berthing operation. In FIGURE 9 it is shown the comparison in case of unberthing operation. Results shows that the contact force its basically independent by the intervention of the GNC, and that the contact force behaviour is similar.
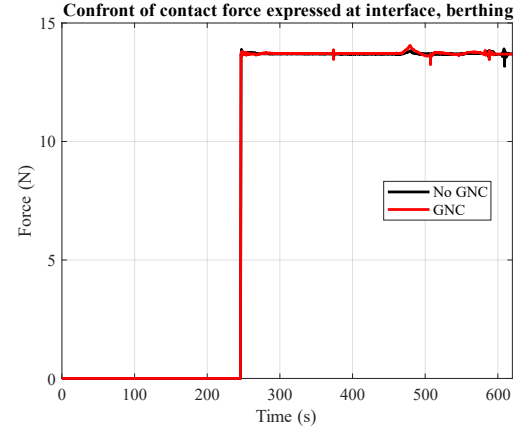

FIGURE 8: CONTACT FORCE COMPARISON FOR BERTHING OPERATION BETWEEN GNC INTERVENTION OR ITS ABSENCE
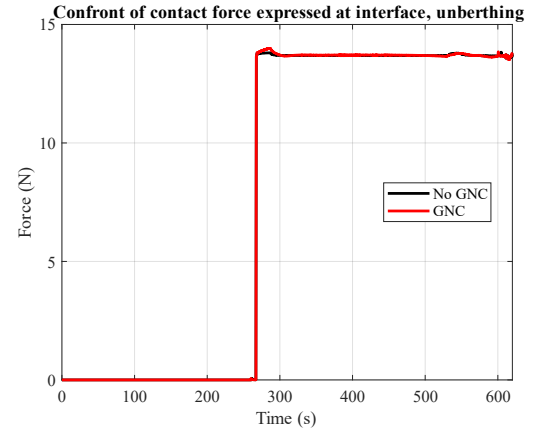

FIGURE 9: CONTACT FORCE COMPARISON FOR UNBERTHING OPERATION BETWEEN GNC INTERVENTION OR ITS ABSENCE

In FIGURE 10 and FIGURE 11 is highlighted the behaviour of the contact force during the approaching of contact surfaces. It can be seen that the behaviour is smooth, meaning that the contact model parameters are correctly chosen.
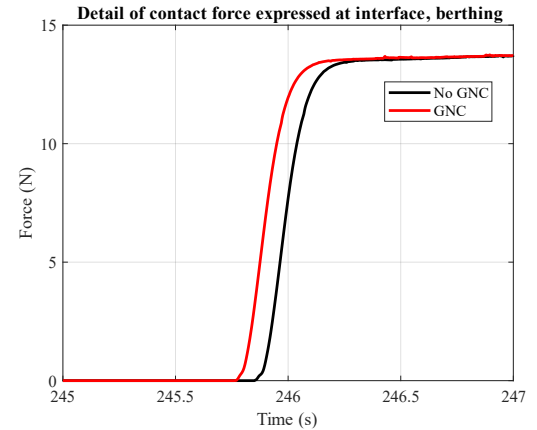

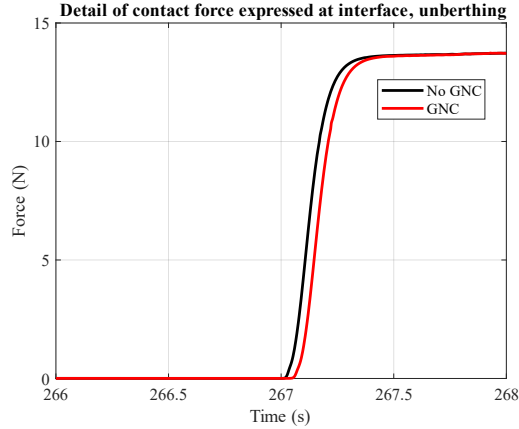**FIGURE 10:** DETAIL OF CONTACT FORCE EXPRESSED AT INTERFACE, BERTHING

FIGURE 11: DETAIL OF CONTACT FORCE EXPRESSED AT INTERFACE, UNBERTHING

In FIGURE 12 and FIGURE 13 it is shown the comparison of energy consumed by the manipulator during the berthing and unberthing. It can be seen that the energy consumption of the manipulator is minorly affected by the intervention of the GNC, while the main energy consumption is due the movement of the target satellite and of the internal dissipation of the robot due to joint friction.
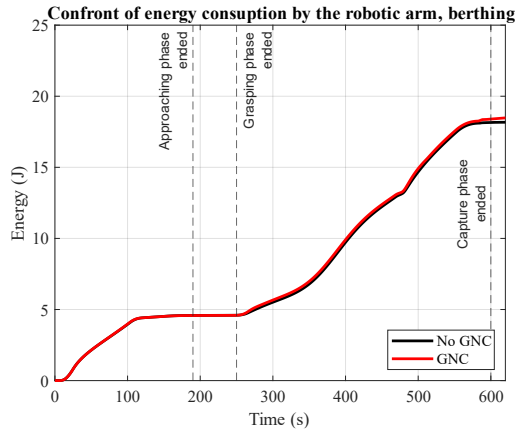

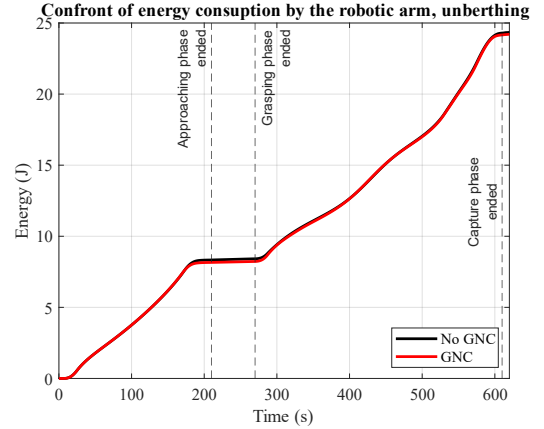**FIGURE 12:** ENERGY CONSUMPTION OF THE ROBOTIC ARM DURING BERTHING MANEUVER

FIGURE 13: ENERGY CONSUMPTION OF THE ROBOTIC ARM DURING THE UNBERTHING MANEUVER

In FIGURE 14 it is reported the energy consumption of the GNC system during the maneuver. In the multibody model the GNC has been introduced as a second order dynamic system, the energy has been computed has the work done by the GNC on the servicer system. It can be seen how the GNC consumption behave during the maneuver, with a total energy consumption of 0.31J for the berthing operation, 0.22J for the unberthing.
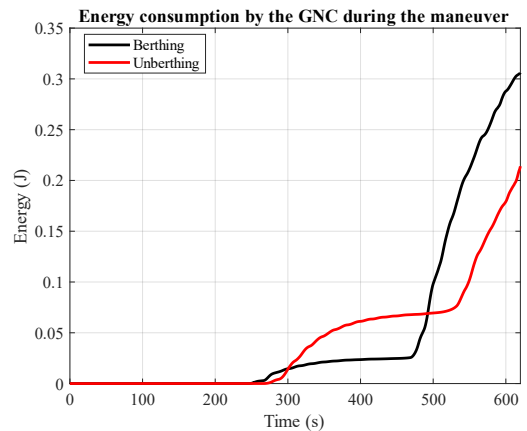

FIGURE 14: ENERGY CONSUMPTION BY THE GNC SYSTEM DURING THE MANEUVER

In FIGURE 15 and FIGURE 16 is reported the behavior of residual angular velocities on the servicer due to the absence of GNC. It can be seen that for both berthing and unberthing the servicer maintain a drift angular velocity of about 10^{-4} rad/s.
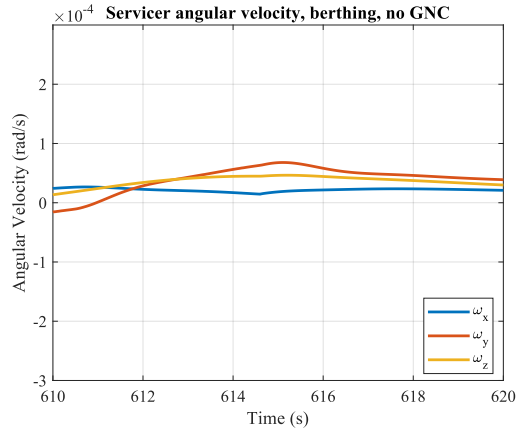
6

FIGURE 15: DETAIL OF THE DRIFT ANGULAR VELOCITIES OF THE SERVICER DUE TO THE ABSENCE OF THE GNC, BERTHING
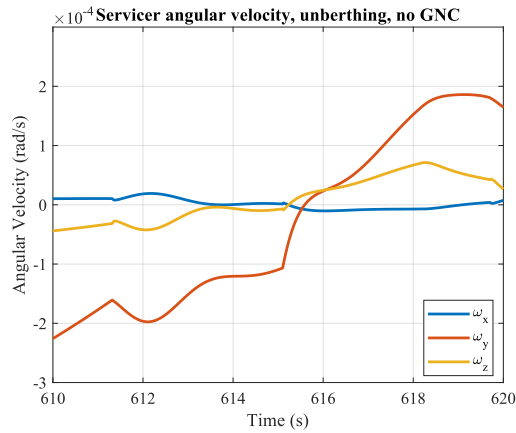

FIGURE 16: DETAIL OF THE DRIFT ANGULAR VELOCITIES OF THE SERVICER DUE TO THE ABSENCE OF THE GNC, UNBERTHING

FIGURE 17 and FIGURE 18 shows the constraint forces and torques reaction at the base of the robot during the berthing maneuver. The peaks in forces and torques coincides with the start and the end of the robot motion. Similar behaviour can be observed during the unberthing maneuver, FIGURE 19 and FIGURE 20. This information can be useful in future work to introduce different control strategies of the robotic arm with the aim of minimizing the constraint reaction, which results in reducing the drift angular velocities on the servicer and the energy consumption of the GNC.
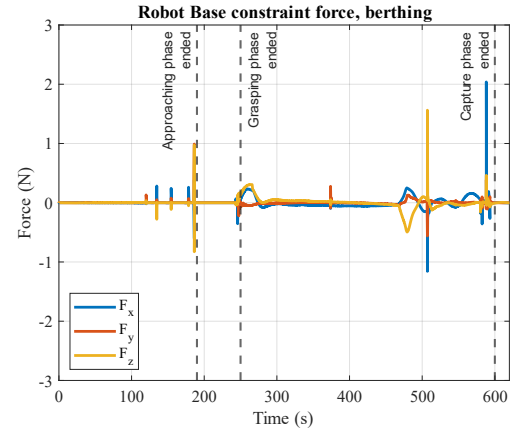

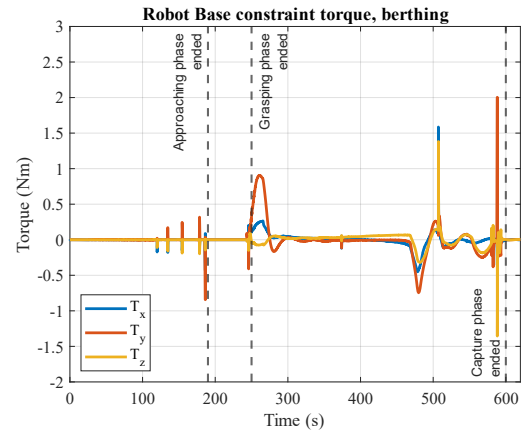**FIGURE 17:** CONSTRAINT REACTION FORCE AT THE ROBOT BASE, BERTHING

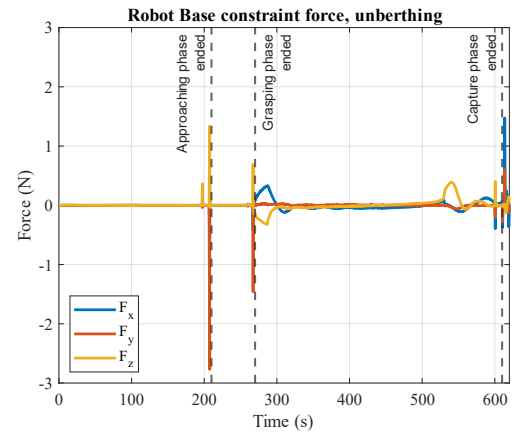**FIGURE 18:** CONSTRAINT REACTION TORQUE AT THE ROBOT BASE, BERTHING

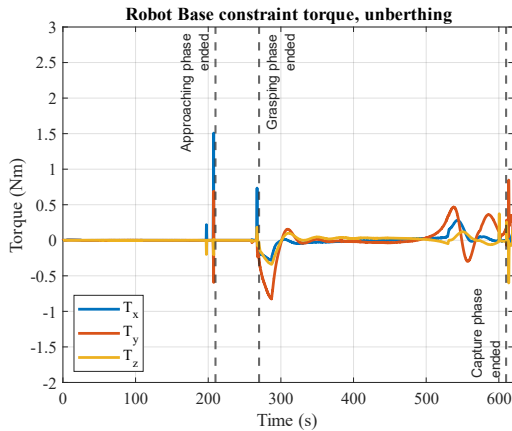**FIGURE 19:** CONSTRAINT REACTION FORCE AT THE ROBOT BASE, UNBERTHING

FIGURE 20: CONSTRAINT REACTION TORQUE AT THE ROBOT BASE, UNBERTHING

4. CONCLUSION

This work presents an analysis of how a robotic arm performs during release and capture operations in multi-satellite mission scenario. It is presented the design of the end effector provided with a gripper feature. Particular attention has been devoted to the description of the contact mechanics between end effector and target interface to allow to simulate a complete maneuver. It has been developed a simulation tool in a multibody environment comprehensive of the two satellites and the physical model of the robotic arm and its control strategy. simulation results allows to verify the capability of the robotic system proposed to perform the capture and release of the target, evaluating the energy consumption of the manipulator and of the GNC in case of its intervention.

REFERENCES

[1] E. Papadopoulos, F. Aghili, O. Ma, and R. Lampariello, "Robotic Manipulation and Capture in Space: A Survey," *Frontiers in Robotics and AI*, vol. 8. Frontiers Media S.A., Jul. 19, 2021. doi: 10.3389/frobt.2021.686723.

[2] A. Flores-Abad, O. Ma, K. Pham, and S. Ulrich, "A review of space robotics technologies for on-orbit servicing," *Progress in Aerospace Sciences*, vol. 68. Elsevier Ltd, pp. 1–26, 2014. doi: 10.1016/j.paerosci.2014.03.002.

[3] Canadian Space Agency, "About Canadarm," https://www.asc-csa.gc.ca/eng/ canadarm/about.asp.

[4] Canadian Space Agency, "About Canadarm 2," https://www.asc-csa.gc.ca/eng/ iss/canadarm2/about.asp.

[5] European Space Agency, "European Robotic Arm," https://www.esa.int/Science_Exploration/Human_and_ Robotic_Exploration/International_Space_Station/Euro pean_Robotic_Arm.

[6] P. Laryssa *et al.*, "International Space Station Robotics: A Comparative Study of ERA, JEMRMS and MSS."

[7] B. Franklin, "On-Orbit Satellite Servicing Study Project Report 'Energy and persistence conquer all things.,'" 2010.

[8] D. Arney, J. Mulvaney, C. Williams, R. Sutherland, and C. Stockdale, "In-space Servicing, Assembly, and Manufacturing (ISAM) State of Play 2022 Edition."

[9] NASA, "OSAM-1 Mission," https://www.nasa.gov/mission/on-orbit-servicing-assembly-and-manufacturing-1/.

[10] NASA's Goddard Space Flight Center, "NASA's Robotic OSAM-1 Mission," https://www.nasa.gov/centers-and-facilities/goddard/nasas-robotic-osam-1-mission-completes-its-critical-design-review/.

[11] "FINAL REPORT OF THE OSAM-1 INDEPENDENT REVIEW BOARD 29 FEBRUARY 2024 Background." [Online]. Available: https://sed.gsfc.nasa.gov/etd/583/tech/asist.

[12] NASA, "OSAM-2 Mission," https://www.nasa.gov/mission/on-orbit-servicing-assembly-and-manufacturing-2-osam-2/.

[13] E. Tunstel, C. Thayer, B. Hayashi, and R. Saltus, "ModuLink: A Robotic Manipulation Applique for In-Space Servicing Vehicles," in *IEEE Aerospace Conference Proceedings*, IEEE Computer Society, 2023. doi: 10.1109/AERO55745.2023.10115712.

[14] P. Palmieri, M. Gaidano, M. Troise, L. Salamina, A. Ruggeri, and S. Mauro, "A deployable and inflatable robotic arm concept for aerospace applications," in *2021 IEEE International Workshop on Metrology for AeroSpace, MetroAeroSpace 2021 - Proceedings*, Institute of Electrical and Electronics Engineers Inc., Jun. 2021, pp. 453–458. doi: 10.1109/MetroAeroSpace51421.2021.9511654.

[15] P. Palmieri, M. Gaidano, A. Ruggeri, L. Salamina, M. Troise, and S. Mauro, "An Inflatable Robotic Assistant for Onboard Applications," in *Proceedings of the International Astronautical Congress, IAC*, International Astronautical Federation, IAF, 2021.

[16] X. L. Ding, Y. C. Wang, Y. B. Wang, and K. Xu, "A review of structures, verification, and calibration technologies of space robotic systems for on-orbit servicing," *Science China Technological Sciences*, vol. 64, no. 3. Springer Verlag, pp. 462–480, Mar. 01, 2021. doi: 10.1007/s11431-020-1737-4.

[17] S. Wu, F. Mou, Q. Liu, and J. Cheng, "Contact dynamics and control of a space robot capturing a tumbling

object," *Acta Astronaut*, vol. 151, pp. 532–542, Oct. 2018, doi: 10.1016/j.actaastro.2018.06.052.

[18] A. Stolfi, P. Gasbarri, and A. K. Misra, "A two-arm flexible space manipulator system for post-grasping manipulation operations of a passive target object," *Acta Astronaut*, vol. 175, pp. 66–78, Oct. 2020, doi: 10.1016/j.actaastro.2020.04.045.

[19] K. Yoshida, H. Nakanishi, H. Ueno, N. Inaba, T. Nishimaki, and M. Oda, "Dynamics, control and impedance matching for robotic capture of a non-cooperative satellite," *Advanced Robotics*, vol. 18, no. 2, pp. 175–198, 2004, doi: 10.1163/156855304322758015.

[20] G. Gilardi and I. Sharf, "Literature survey of contact dynamics modelling." [Online]. Available: www.elsevier.com/locate/mechmt

[21] W. Cheng, L. Tianxi, and Z. Yang, "Grasping strategy in space robot capturing floating target," *Chinese Journal of Aeronautics*, vol. 23, no. 5, pp. 591–598, Oct. 2010, doi: 10.1016/S1000-9361(09)60259-4.

[22] O. Ma, G. Yang, and X. Diao, "EXPERIMENTAL VALIDATION OF CDT-BASED SATELLITE DOCKING SIMULATIONS USING SOSS TESTBED," 2005.

[23] J. Wang, R. Mukherji, M. Ficocelli, A. Ogilvie, and C. Rice, "Contact dynamics simulations for robotic servicing of Hubble Space Telescope," in *Modeling, Simulation, and Verification of Space-based Systems III*, SPIE, May 2006, p. 622103. doi: 10.1117/12.665348.

[24] Institute of Electrical and Electronics Engineers., *The proceedings of 2006 IEEE/RSJ International Conference on Intelligent Robots and Systems : IROS 2006 : Beijing, China, October 9-15, 2006*.

[25] L. Salamina, D. Botto, S. Mauro, and S. Pastorelli, "Modeling of flexible bodies for the study of control in the simulink environment," *Applied Sciences (Switzerland)*, vol. 10, no. 17, Sep. 2020, doi: 10.3390/app10175861.

[26] "Adams 2020 FP1 Adams View User's Guide," 2020. [Online]. Available: http://msc-documentation.questionpro.com.

[27] C. Verheul and S. International, "Benelux ADAMS User Meeting."

[28] P. Palmieri, M. Troise, L. Salamina, M. Gaidano, M. Melchiorre, and S. Mauro, "An Inflatable 7-DOF Space Robotic Arm for Active Debris Removal," in *Okada, M. (eds) Advances in Mechanism and Machine Science. IFToMM WC 2023. Mechanisms and Machine Science, vol 148*, Springer, Cham, 2023, pp. 580–589. doi: 10.1007/978-3-031-45770-8_58.

[29] P. Palmieri, M. Troise, M. Gaidano, M. Melchiorre, and S. Mauro, "Inflatable Robotic Manipulator for Space Debris Mitigation by Visual Servoing," in *2023 9th International Conference on Automation, Robotics and Applications, ICARA 2023*, Institute of Electrical and Electronics Engineers Inc., 2023, pp. 175–179. doi: 10.1109/ICARA56516.2023.10125753.

[30] B. Siciliano, L. Sciavicco, L. Villani, and G. Oriolo, *Robotics. Modelling, Planning and Control.* 2010.